

https://dspace.org/

Experimentally simulating the beam shaping capabilities of pistontype deformable mirrors using a liquid crystal spatial light modulator

Scholes, Stirling; Mohapi, Lehloa

2023
Springer
https://hdl.handle.net/10539/49535

Downloaded from a DSpace repository. https://dspace.org/

Applied Physics B (2023) 129:45
https://doi.org/10.1007/s00340-023-07991-3

Applied Physics B
Lasers and Optics

RESEARCH

Experimentally simulating the beam shaping capabilities of piston-type deformable mirrors using a liquid crystal spatial light modulator

Stirling Scholes[1] · Lehloa Mohapi[2] · Jonathan Leach[1] · Andrew Forbes[2] · Angela Dudley[2]

Received: 7 November 2022 / Accepted: 15 February 2023 / Published online: 28 February 2023
© The Author(s) 2023

Abstract
The number of mirror segments, mirror geometry and orientation are essential parameters when assessing the beam-shaping capabilities of deformable mirrors. Here, we use a Liquid Crystal on Silicon Spatial Light Modulator (LCoS-SLM) to mimic the mechanical design of a deformable mirror and quantitatively analyse the effect of the number of mirror segments and their geometrical structure on resulting structured modes. Our approach can be used as a test bed prior to designing a deformable mirror for high power beam shaping.

1 Introduction

Adaptive optics with deformable mirrors have predominately been used in astronomy to correct for atmospheric aberrations in order to rectify and produce clearer more visible images [1, 2]. Various types of deformable mirrors exist, the most widely adopted are the bimorph and piston-based deformable mirrors. Bimorph deformable mirrors consist of two poled piezoelectric ceramic wafers, covered with a thin glass membrane that is deformed in order to achieve wavefront control. Piston-based deformable mirrors, classified as segmented deformable mirrors, consist of arrays (of a variety of geometries - square, circular, hexagonal, etc.) of rigid, segmented mirrors [3]. In order to achieve surface deformation with such segmented mirrors, a voltage is applied to each mirror electrode, giving rise to a controlled actuator stroke [4]. Predominately, deformable mirrors have been used in adaptive optics setups to correct for optical aberrations present in incoming wavefronts [5, 6].

Apart from wavefront correction, both forms of deformable mirrors have found applications in beam shaping. Due to their high-power handling capabilities, they are particularly useful for the spatial control of high power beams. These mirrors have been applied to intra-cavity compensation of low-order wavefront aberrations to improve beam quality [7, 8], achieve mode matching [9] and perform fast switching between stable and unstable resonator configurations [10]. It has been shown that these mirrors can be engineered to withstand radiation power densities up to 3 kW/cm^2 for continuous sources and roughly 1010 W/cm^2 for pulsed sources [11]. External to the laser cavity, these deformable mirrors have also shown wavefront correction and distribution compensation with both wide and small aperture mirrors [12–15]. Extending this to spatial-profile control, these mirrors have been demonstrated to produce elliptical and rectangular super-Gaussian and annular beam-shapes [16–18] and Bessel modes via a magnetic fluid-based liquid deformable mirror [19].

Although segmented deformable mirrors cause light to diffract due to the spacing between the segments [20], they are ideal for phase singularity beam shaping since the segments can be individually controlled to reproduce a spiral configuration. For example, Robert et al reported the creation of optical vortices by using an Iris AO S37-X deformable mirror consisting of 37 hexagonal actuators [21], where they formed a discontinuous reflective surface by altering each actuator to form a spiral configuration in a piston-tip-tilt fashion. The topological charge carried by the resulting modes was verified with the use of a Michelson interferometer to produce an interference pattern with a reference plane [22]. The generation of both zero and higher-order

✉ Angela Dudley
angela.dudley@wits.ac.za

[1] School of Engineering and Physical Sciences, Heriot-Watt University, Edinburgh EH14 4AS, UK

[2] School of Physics, University of the Witwatersrand, Private Bag 3, Johannesburg 2050, South Africa

Bessel-Gauss beams have also been reported, whereby a segmented deformable mirror having 37 hexagonal segments in a honeycomb configuration was used. First the deformable mirror was used as a reflective axicon to generate the zero-order Bessel beam, and then it was programmed to produce a 2π spiral phase for the creation of higher-order Bessel beams [23]. However, these spatial modes are often not of a high fidelity (or correlation) with their desired "true" spatial profile. Spatial Light Modulators (SLMs), on the other hand, have been used extensively to produce spatial modes [24–28] of very high-fidelity for a variety of applications. These applications range from mode-division multiplexing [29], quantum information protocols [30–32], advanced adaptive optics systems [33], laser material processing [34–36], and brightness enhancement [37]. The advantage of SLMs is that they span a wide range of wavelengths (from visible through to near-infrared and in some cases mid-infrared), while offering instantaneous and rewritable amplitude, phase and polarization control, allowing for the creation of high-purity modes [38–42], independent wavelength control [43], as well as hundreds of structured modes from a single device [44], ranging from LG [45, 46] HG [17], IG [47], BG [48, 49], azimuthal OAM modes [50, 51] and non-diffracting beams [52, 53]. SLMs have also been applied to intra-cavity beam-shaping [54], as well as interferometrically combining resulting modes to create vector beams [55–59].

Since only a few publications have been dedicated to the implementation of deformable mirrors for low-fidelity beam-shaping, we propose first understanding the effect of the various deformable mirror parameters on the resulting spatial profile capabilities. In order to investigate such, we implement a dynamically addressable technology (in the form of a SLM) to act as a test-bed in simulating the various deformable mirror parameters (as depicted in Fig. 1). SLMs are well suited to this task since their discrete pixel arrangement and finite number of phase steps is exactly analogous to the discrete number of mirror segments and finite actuator positions associated with deformable mirrors. Here, we investigate the effect the mirror segment arrangement [such as, the number of mirror segments and their geometrical orientation (namely, Cartesian or radial)] has on the fidelity of the resulting structured mode. This assists in accelerating the decision-making process in determining which deformable mirror arrangement is best suited to achieve the desired spatial profile.

2 Theory and experimental realization

Figure 1 illustrates the conceptual implementation of the experimental simulator. An ideal phase profile, (shown in Fig. 1 as $\exp(i\ell\phi)$ with $\ell = 3$) is divided into N segments of arbitrary geometry with each segment corresponding to a single simple linear actuator within the deformable mirror array. Each actuator is assumed to have a stroke S and precision p allowing for a total phase modulation (in reflection) of $4\pi S/\lambda$ in S/p discrete steps (where λ is the wavelength of the illuminating light). Each region of the segmented phase profile is assigned a value from the list of S/p allowed actuator positions which results in a phase nearest the average value of the region. The discretized phase map is converted to a phase only hologram and displayed on an SLM.

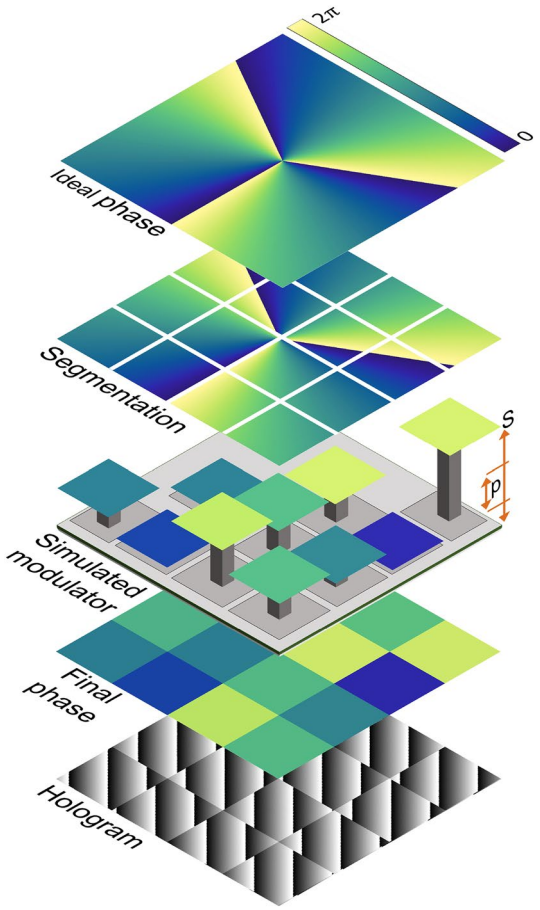


Fig. 1 The modulator simulation process depicted conceptually. The ideal phase profile is divided into a given number of segments according to the selected geometry. Each segment is assigned the nearest allowed phase based on the simulated modulators actuator stroke S and actuator precision p. The final phase map, discretized both transversely and in amplitude, is converted to a phase only hologram and displayed on an SLM

To quantify the impact of segment number and geometry on beam quality we define a Figure of Merit (FoM) as:

$$\mathrm{FoM} = \frac{\sum\left(I_0^r - \bar{I}_0^r\right)\left(I_m^r - \bar{I}_m^r\right)}{\sqrt{\sum\left(I_0^r - \bar{I}_0^r\right)^2 \sum\left(I_m^r - \bar{I}_m^r\right)^2}} \times \frac{\sum I_m^r}{\sum I_0^r}, \tag{1}$$

where I_0^r and I_m^r are the desired and measured intensity profiles within a region of interest r. $\sum$ represents the sum over all coordinates and, $\bar{I}_0^r$ and $\bar{I}_m^r$ are the average intensities. The first term of Eqn. 1 defines the transverse correlation between the measured and desired intensity profiles within some region r. The second term defines the efficiency i.e., the ratio between the ideal and measured total energy within the region of interest. A deformable mirror capable of perfect beam shaping would result in beams with a FoM of 1.

Figure 2 depicts the effect of segment stroke S and segment number on Eq. 1 for a vortex beam with $\ell = 3$. As the stroke of each segment is increased from 0.25λ to 0.5λ (effectively increasing the modulation from π to 2π) the FoM improves, as indicated by the plot corresponding to the dashed red trace line (Fig. 2B). This is further illustrated by comparing Figs. 2E and D. In Fig. 2E, the limited stroke S of the modulator is unable to produce the required phase (despite the relatively large segment number) resulting in an output which is essentially unmodulated. Additionally, the FoM improves as the number of transverse segments comprising the modulator increases (Fig. 2A). Figure 2C shows that for low segment numbers near $S = 0.5\lambda$ the modulator is able to introduce an optical vortex, but the final beam remains highly distorted. Together these findings are consistent with the intuition that the highest fidelity beam shaping (Fig. 2D) is achieved by modulators with at least a 2π modulation capability and a large number of transverse segments.

An advantage of our approach is its ease of implementation as shown conceptually in Fig. 3. The SLM (a HoloEye Pluto 2) is illuminated by a Gaussian beam from a HeNe laser with the beam being sufficiently small so as to avoid the edges of the hologram. The first order diffraction is passed through a lens of focal length $f = 500$ mm and the resultant intensity profile recorded by a Spiricon SP300 camera at the focal plane. For the remainder of this work, we assign values of 5 μm and 1 nm to S and p, respectively, in line with commercially available devices, and assume independent modulator segments.

In the following section we examine the effect of segment number and geometry on the FoM for a selection of transverse beam profiles specifically, a Cartesian flattop, an Orbital Angular Momentum (OAM) free annular, and, an $\ell = 3$ vortex beam.

3 Results and discussion

Figure 4 illustrates how as the number of transverse segments comprising the modulator increases so too does the figure of merit. At low segment numbers the modulators ability to reproduce complex phase profiles is limited as evidenced by the aliasing in the left most phase panel of Fig. 4. This aliasing both directs energy away from the

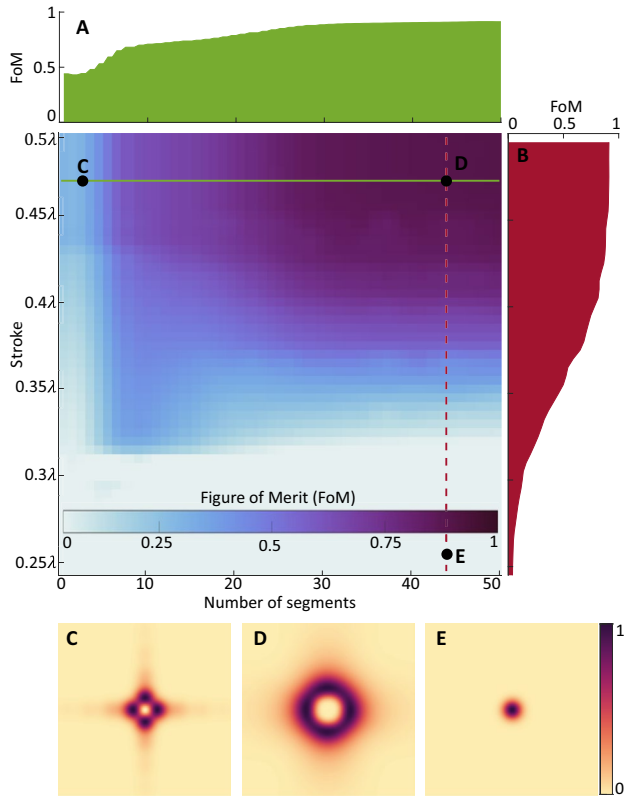


Fig. 2 Eq. 1 as a function of the segment stroke S and the number of segments for a vortex beam with $\ell = 3$. The subpanels A and B illustrate the trace of Eqn. 1 along each axis at the positions indicated by the solid green and red dashed lines respectively. C, D, and E, show the simulated transverse intensity profiles of the modulated beam at the points indicated in the density plot

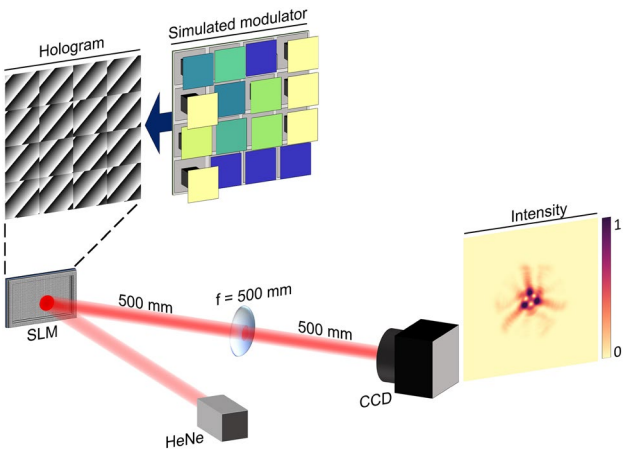


Fig. 3 The experimental setup depicted conceptually for the case of a 4×4 Cartesian modulator. The hologram representing the modulator is displayed on an SLM illuminated by a Gaussian beam from a HeNe laser. The first order diffraction is passed through a lens of focal length f and the resultant intensity profile recorded by a camera at the focal plane

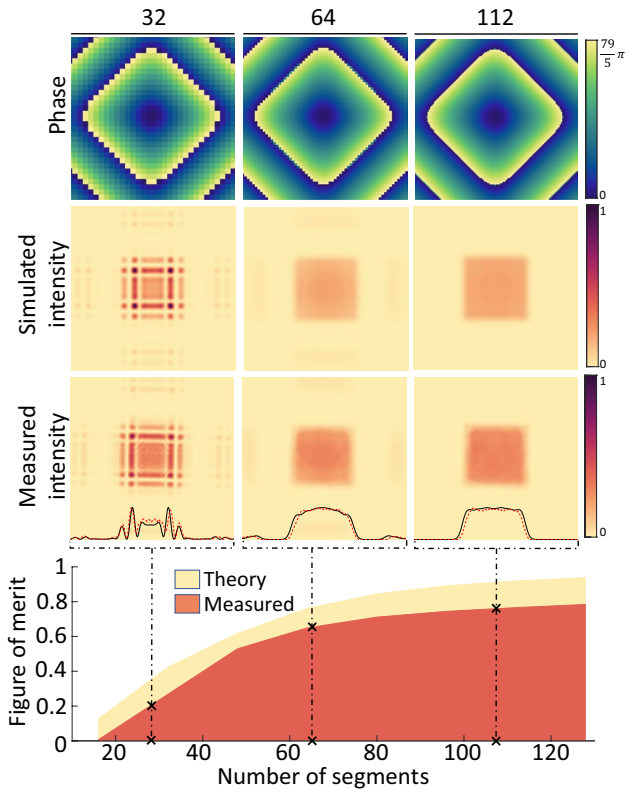


Fig. 4 The influence of the number of mirror segments on the figure of merit. The theoretical and measured results are shown as solid black and red dashed lines respectively. The offset between the two curves is due to the limited dynamic range of the camera and can be accounted for using a constant offset correction of 0.13. The top panels illustrate the measured intensity and hologram phase at the locations indicated by the risers, 32, 64, and, 112 transverse segments respectively. The lines in the intensity panels illustrate the agreement in the transverse structure between the measured (red dashed) and simulated (solid black) beams

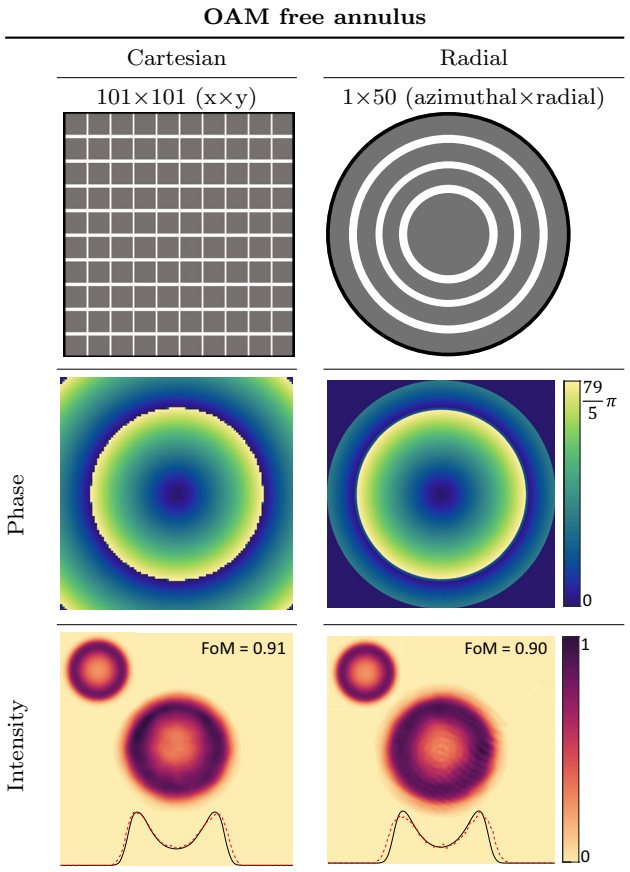


Fig. 5 The minimum number of segments required to produce an OAM free annulus with a FoM ≥ 90% in the Cartesian (left) and radial (right) arrangements. The top row illustrates the relevant segment geometry, note that the number of segments depicted has been reduced to aid in visualisation. The middle row shows the ideal phase profile when mapped to the segments in each configuration. The bottom row shows the measured intensity profile with the insets in the upper corner showing the ideal beam profile. The text indicates the FoM for each beam. The lines in the intensity panels illustrate the agreement in the transverse structure between the measured (red dashed) and simulated (solid black) beams

region of interest and distorts the transverse intensity profile of the beam resulting in a low figure of merit. As the number of segments is increased (and the phase profile better approximated), the fidelity of the beam within the region of interest increases while the energy lost to side lobes decreases, resulting in a figure of merit which asymptotically approaches one.

Figure 5 illustrates that the number of modulator segments required to achieve a beam with a specific FoM is contingent on the compatibility between the segment geometry and the phase profile. Specifically, modulators having segment geometries which match the underlying phase profile can produce beams of either, comparable quality with fewer segments, or, higher quality with the same number of segments. In the Cartesian configuration, although the final FoM is slightly higher, a large number of segments (101× 101) are required to reduce the aliasing in the phase (Fig. 5 middle row left panel) to acceptable levels. By contrast, since the desired phase profile is radially symmetric, a modulator comprised of only concentric rings is able to accurately reproduce the phase profile with a relatively low number of total segments (50 concentric rings).

To further examine the effect of segment geometry a second radially symmetric case (depicted in Fig. 6) was considered. Specifically, a modulator with 50 radial segments (as with the radial case in Fig. 5) was constructed however, each radial segment was further divided into a number of azimuthal segments. The inner most disk of the modulator comprised 9 azimuthal segments with the number of azimuthal segments per concentric ring increasing linearly towards the perimeter of the modulator. The ability of this modulator to produce a vortex beam (with $\ell = 3$) is depicted in Fig. 6.

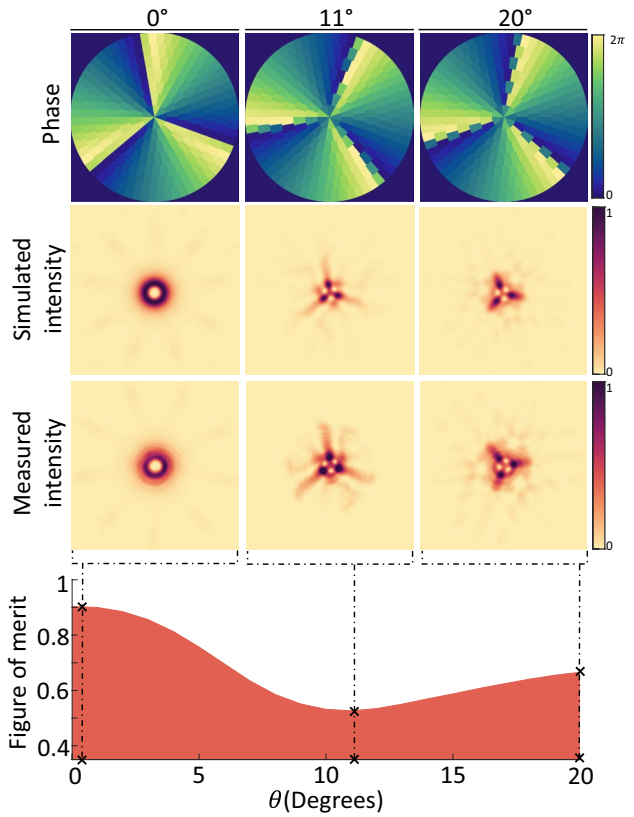


Fig. 6 The effect of rotating the phase profile of a vortex beam (with $\ell = 3$) on the FoM. As the phase profile is rotated through θ, the discontinuities in the phase profile move into (and out of) alignment with the discontinuities between segments changing the degree of aliasing in the phase profile and by extension the FoM of the measured beam. The top panels illustrate the measured intensity and phase (mapped to the segments) at the locations indicated by the risers, 0°, 11°, and, 20° respectively. Note that the intensity panels have been independently normalized to aid in visualization

There are two important findings contained in Fig. 6. First, whilst the vortex and OAM free annular beams (Fig. 5) have comparable radial symmetry in their intensity profiles, the azimuthal discontinuities in the phase of the vortex beam necessitate the use of a modulator with at least some degree of azimuthal control. This further highlights that the ability of a modulator to produce a given beam type is closely related to the compatibility between the segment geometry and the underlying phase profile, rather than the ultimate intensity distribution. Second, the alignment of phase discontinuities with discontinuities between the modulator segments can have a significant impact on the FoM of the final beam. Figure 6 illustrates how as the phase profile for the vortex beam (with $\ell = 3$) is rotated the discontinuities in the phase profile move into (and out of) alignment with the discontinuities between segments. This alignment then changes the degree of aliasing in the phase profile and by extension the FoM of the measured beam. This effect is cyclic with a periodicity controlled by the relationship between the number of azimuthal segments in the modulator and the number of discontinuities in the phase profile. We stress that whilst we have demonstrated this effect for radial geometries, it can be readily extended to any combination of phase profile and segment structures. Further, the effect emphasises how careful selection, and implementation, of modulator geometries is key in realising high quality structured beams from modulators with limited (often low) numbers of segments.

4 Conclusion

We have examined how the ability of a segmented deformable mirror to produce structured beams is impacted by the number of mirror segments it comprises as well as by their geometry. We have demonstrated a simple and flexible deformable mirror simulator (based on an LCoS-SLM) capable of producing beams in close agreement with theoretical predictions. Finally, we have highlighted the importance of the compatibility between the segment structure and the underlying phase profile of the desired beam. We expect this work to be a valuable reference point for the implementation of deformable mirrors in the context of high power structured light.

Acknowledgements AD acknowledges funding from the DSI-CSIR Rentalpool programme.

Funding Open access funding provided by University of the Witwatersrand.

Data availability The datasets generated and analyzed during the current study are available from the corresponding author on reasonable request.

Open Access This article is licensed under a Creative Commons Attribution 4.0 International License, which permits use, sharing, adaptation, distribution and reproduction in any medium or format, as long as you give appropriate credit to the original author(s) and the source, provide a link to the Creative Commons licence, and indicate if changes were made. The images or other third party material in this article are included in the article's Creative Commons licence, unless indicated otherwise in a credit line to the material. If material is not included in the article's Creative Commons licence and your intended use is not permitted by statutory regulation or exceeds the permitted use, you will need to obtain permission directly from the copyright holder. To view a copy of this licence, visit http://creativecommons.org/licenses/by/4.0/.

References

1. F. Roddier, Adaptive optics in astronomy. Rev. Laser Eng. **27**(2), 78–83 (1999)
2. R.K. Tyson, B.W. Frazier, *Principles of adaptive optics* (CRC Press, 2022)

3. R. Freeman, J.E. Pearson, Deformable mirrors for all seasons and reasons. Appl. Opt. **21**(4), 580 (1982)
4. M.C. Roggemann, V.M. Bright, B.M. Welsh, S.R. Hick, P.C. Roberts, W.D. Cowan, J.H. Comtois, Use of micro-electro-mechanical deformable mirrors to control aberrations in optical systems: theoretical and experimental results. Opt. Eng. **36**(5), 1326 (1997)
5. L. Hu, L. Xuan, Y. Liu, Z. Cao, D. Li, Q. Mu, Phase-only liquid-crystal spatial light modulator for wave-front correction with high precision. Opt. Exp. **12**(26), 6403 (2004)
6. H. Ma, Z. Liu, H. Wu, X. Xu, J. Chen, Adaptive correction of vortex laser beam in a closed-loop system with phase only liquid crystal spatial light modulator. Opt. Commun. **285**(6), 859 (2012)
7. A.V. Kudryashov, V.V. Samarkin, Control of high power co2 laser beam by adaptive optical elements. Opt. Commun. **118**(3–4), 317 (1995)
8. S. Piehler, B. Weichelt, A. Voss, M.A. Ahmed, T. Graf, Power scaling of fundamental-mode thin-disk lasers using intracavity deformable mirrors. Opt. Lett. **37**(24), 5033 (2012)
9. J.D. Mansell, R.L. Byer, Micromachined silicon deformable mirror. Adapt. Opt. Syst. Technol. SPIE. **3353**, 896–901 (1998)
10. G. Vdovin, V. Kiyko, Intracavity control of a 200-w continuous-wave nd: Yag laser by a micromachined deformable mirror. Opt. Lett. **26**(11), 798 (2001)
11. V. Samarkin, V. Zavalova, A. Alexandrov, A. Roukossouev, A. Kudryashov: In *2003 Conference on Lasers and Electro-Optics Europe (CLEO/Europe 2003)(IEEE Cat. No. 03TH8666)* (IEEE, 2003), p. 107
12. A. Kudryashov, V. Samarkin, A. Alexandrov, J. Sheldakova, P. Romanov, In Laser Resonators. Microresonators Beam Cont. XVI. **8960**, 198–203 (2014)
13. N. Lefaudeux, X. Levecq, L. Escolano, S. Theis, Large deformable mirrors for beam control of high brightness lasers. Laser Res. Microresonators Beam Cont. XV. **8600**, 116–121 (2013)
14. S. Li, L. Zhou, C. Cui, K. Wang, X. Yan, Y. Wang, L. Ding, Y. Wang, Z. Lu, Wavefront shaping by a small-aperture deformable mirror in the front stage for high-power laser systems. Appl. Sci. **7**(4), 379 (2017)
15. J.C. Dainty, A.V. Koryabin, A.V. Kudryashov, Low-order adaptive deformable mirror. Appl. Opt. **37**(21), 4663 (1998)
16. B.G. Henderson, J.D. Mansell, Advanced Wavefront Control: Methods, Devices, and Applications VI. Advan. Wavefront Cont. Methods Devices Appl. VI. **7093**, 123–132 (2008)
17. J.D. Mansell, B.G. Henderson, G. Robertson, in Advanced Wavefront Control: Methods, Devices, and Applications VIII, Evaluation of polymer membrane deformable mirrors for high peak power laser machining applications, vol 7816 (SPIE, 2010), pp. 151–164
18. S. Sinha, J.D. Mansell, R.L. Byer, Deformable mirrors for high-power laser. High-Resol. Wavefront Cont. MethodsDev. Appl. III. **4493**, 55–63 (2002)
19. Z.Z. Wu, Z. Zhang, X.H. Kong, J.Q. Wu, T. Wang, M. Liu, S.R. Xie, Laser beam shaping with magnetic fluid-based liquid deformable mirrors. Chin. Phys. B **26**(7), 074201 (2017)
20. A. Tuantranont, V.M. Bright, Segmented silicon-micromachined microelectromechanical deformable mirrors for adaptive optics. IEEE J. Select. Top. Quantum Electron. **8**(1), 33 (2002)
21. M.A. Helmbrecht, T. Juneau, M. Hart, N. Doble, Segmented MEMS deformable-mirror technology for space application. Micro (MEMS) Nanotechnol. Space Appl. **6223**, 25 (2006)
22. R.K. Tyson, M. Scipioni, J. Viegas, Generation of an optical vortex with a segmented deformable mirror. Appl. Opt. **47**(33), 6300 (2008)
23. X. Yu, A. Todi, H. Tang, Bessel beam generation using a segmented deformable mirror. Appl. Opt. **57**(16), 4677 (2018)
24. H. Rubinsztein-Dunlop, A. Forbes, M.V. Berry, M.R. Dennis, D.L. Andrews, M. Mansuripur, C. Denz, C. Alpmann, P. Banzer, T. Bauer et al., Roadmap on structured light. J. Opt. **19**(1), 013001 (2016)
25. C. Rosales-Guzmán, A. Forbes, *How to shape light with spatial light modulators* (SPIE Press, 2017)
26. G. Lazarev, P.J. Chen, J. Strauss, N. Fontaine, A. Forbes, Beyond the display: phase-only liquid crystal on silicon devices and their applications in photonics. Opt. Exp. **27**(11), 16206 (2019)
27. A. Forbes, A. Dudley, M. McLaren, Creation and detection of optical modes with spatial light modulators. Advan. Opt. Photon. **8**(2), 200 (2016)
28. S. Scholes, V. Rodríguez-Fajardo, A. Forbes, Lossless reshaping of structured light. JOSA A **37**(11), C80 (2020)
29. M. Salsi, C. Koebele, D. Sperti, P. Tran, H. Mardoyan, P. Brindel, S. Bigo, A. Boutin, F. Verluise, P. Sillard et al., Mode-division multiplexing of 2×100 gb/s channels using an lcos-based spatial modulator. J. Lightwave Technol. **30**(4), 618 (2011)
30. M.T. Gruneisen, W.A. Miller, R.C. Dymale, A.M. Sweiti, Holographic generation of complex fields with spatial light modulators: application to quantum key distribution. Appl. Opt. **47**(4), A32 (2008)
31. X. Sun, I.B. Djordjevic, M.A. Neifeld, Multiple spatial modes based qkd over marine free-space optical channels in the presence of atmospheric turbulence. Opt. Exp. **24**(24), 27663 (2016)
32. Z.X. Li, Y.P. Ruan, P. Chen, J. Tang, W. Hu, K.Y. Xia, Y.Q. Lu, Liquid crystal devices for vector vortex beams manipulation and quantum information applications. Chin. Opt. Lett. **19**(11), 112601 (2021)
33. R. Grunwald, M. Jurke, M. Bock, M. Liebmann, B.P. Bruno, H. Gowda, U. Wallrabe, Photons. **9**, 42 (2022)
34. N. Sanner, N. Huot, E. Audouard, C. Larat, J.P. Huignard, Direct ultrafast laser micro-structuring of materials using programmable beam shaping. Opt. Lasers Eng. **45**(6), 737 (2007)
35. Z. Kuang, W. Perrie, J. Leach, M. Sharp, S.P. Edwardson, M. Padgett, G. Dearden, K.G. Watkins, High throughput diffractive multi-beam femtosecond laser processing using a spatial light modulator. Appl. Surf. Sci. **255**(5), 2284 (2008)
36. D. Flamm, D.G. Grossmann, M. Sailer, M. Kaiser, F. Zimmermann, K. Chen, M. Jenne, J. Kleiner, J. Hellstern, C. Tillkorn et al., Structured light for ultrafast laser micro-and nanoprocessing. Opt. Eng. **60**(2), 025105 (2021)
37. S. Scholes, A. Forbes, Improving the beam quality factor (m 2) by phase-only reshaping of structured light. Opt. Lett. **45**(13), 3753 (2020)
38. A. Jesacher, C. Maurer, A. Schwaighofer, S. Bernet, M. Ritsch-Marte, Full phase and amplitude control of holographic optical tweezers with high efficiency. Opt. Exp. **16**(7), 4479 (2008)
39. A. Jesacher, C. Maurer, A. Schwaighofer, S. Bernet, M. Ritsch-Marte, Near-perfect hologram reconstruction with a spatial light modulator. Opt. Exp. **16**(4), 2597 (2008)
40. T.W. Clark, R.F. Offer, S. Franke-Arnold, A.S. Arnold, N. Radwell, Comparison of beam generation techniques using a phase only spatial light modulator. Opt. Exp. **24**(6), 6249 (2016)
41. N. Radwell, R.F. Offer, A. Selyem, S. Franke-Arnold, Optimisation of arbitrary light beam generation with spatial light modulators. J. Opt. **19**(9), 095605 (2017)
42. D. Bowman, T.L. Harte, V. Chardonnet, C. De Groot, S.J. Denny, G. Le Goc, M. Anderson, P. Ireland, D. Cassettari, G.D. Bruce, High-fidelity phase and amplitude control of phase-only computer generated holograms using conjugate gradient minimisation. Opt. Exp. **25**(10), 11692 (2017)
43. D.M. Spangenberg, A. Dudley, P.H. Neethling, E.G. Rohwer, A. Forbes, White light wavefront control with a spatial light modulator. Opt. Exp. **22**(11), 13870 (2014)

44. C. Rosales-Guzmán, N. Bhebhe, N. Mahonisi, A. Forbes, Multiplexing 200 spatial modes with a single hologram. J. Opt. **19**(11), 113501 (2017)
45. Y. Ohtake, T. Ando, N. Fukuchi, N. Matsumoto, H. Ito, T. Hara, Universal generation of higher-order multiringed laguerre-gaussian beams by using a spatial light modulator. Opt. Lett. **32**(11), 1411 (2007)
46. T. Ando, Y. Ohtake, N. Matsumoto, T. Inoue, N. Fukuchi, Mode purities of laguerre-gaussian beams generated via complex-amplitude modulation using phase-only spatial light modulators. Opt. Lett. **34**(1), 34 (2009)
47. J.B. Bentley, J.A. Davis, M.A. Bandres, J.C. Gutiérrez-Vega, Generation of helical ince-gaussian beams with a liquid-crystal display. Opt. Lett. **31**(5), 649 (2006)
48. R. Vasilyeu, A. Dudley, N. Khilo, A. Forbes, Generating superpositions of higher-order bessel beams. Opt. Exp. **17**(26), 23389 (2009)
49. I. Moreno, J.A. Davis, M.M. Sánchez-López, K. Badham, D.M. Cottrell, Nondiffracting bessel beams with polarization state that varies with propagation distance. Opt. Lett. **40**(23), 5451 (2015)
50. N. Heckenberg, R. McDuff, C. Smith, A. White, Generation of optical phase singularities by computer-generated holograms. Opt. Lett. **17**(3), 221 (1992)
51. S. Franke-Arnold, L. Allen, M. Padgett, Advances in optical angular momentum. Laser Photons. Rev. **2**(4), 299 (2008)
52. C. López-Mariscal, K. Helmerson, Shaped nondiffracting beams. Opt. Lett. **35**(8), 1215 (2010)
53. H. Ma, Z. Liu, P. Zhou, X. Wang, Y. Ma, X. Xu, Generation of flat-top beam with phase-only liquid crystal spatial light modulators. J. Opt. **12**(4), 045704 (2010)
54. A. Forbes, Structured light from lasers. Laser Photons. Rev. **13**(11), 1900140 (2019)
55. M.A. Neil, F. Massoumian, R. Juškaitis, T. Wilson, Method for the generation of arbitrary complex vector wave fronts. Opt. Lett. **27**(21), 1929 (2002)
56. C. Maurer, A. Jesacher, S. Fürhapter, S. Bernet, M. Ritsch-Marte, Tailoring of arbitrary optical vector beams. New J. Phys. **9**(3), 78 (2007)
57. S. Franke-Arnold, J. Leach, M.J. Padgett, V.E. Lembessis, D. Ellinas, A.J. Wright, J.M. Girkin, P. Öhberg, A.S. Arnold, Optical ferris wheel for ultracold atoms. Opt. Exp. **15**(14), 8619 (2007)
58. C. Rosales-Guzmán, N. Bhebhe, A. Forbes, Simultaneous generation of multiple vector beams on a single slm. Opt. Exp. **25**(21), 25697 (2017)
59. N. Bhebhe, P.A. Williams, C. Rosales-Guzmán, V. Rodriguez-Fajardo, A. Forbes, A vector holographic optical trap. Sci. Rep. **8**(1), 1 (2018)

Publisher's Note Springer Nature remains neutral with regard to jurisdictional claims in published maps and institutional affiliations.